GEOPHYSICS, VOL. 68, NO. 1 (JANUARY-FEBRUARY 2003); P. 337–345, 10 FIGS., 1 TABLE.
10.1190/1.1543219

Quantifying the effectiveness of stabilized inverse *Q* filtering

Yanghua Wang*

ABSTRACT

Applying inverse *Q* filtering to surface seismic data may minimize the effect of dispersion and attenuation and hence improve the seismic resolution. In this case study, a stabilized inverse *Q* filter is applied to a land seismic data set, for which the prerequisite reliable earth *Q* function is estimated from the vertical seismic profile (VSP) downgoing wavefield. The paper focuses on the robust estimate of *Q* values from VSP data and on the quantitative evaluation of the effectiveness of the stabilized inverse *Q* filtering approach. The quantitative evaluation shows that inverse *Q* filtering may flatten the amplitude spectrum, strengthen the time-variant amplitude, increase the spectral bandwidth, and improve the signal-to-noise (S/N) ratio. A parameter measuring the resolution enhancement is defined as a function of the changes in the bandwidth and the S/N ratio. The stabilized inverse *Q* filtering algorithm, which may provide a stable solution for compensating the high-frequency wave components lost through attenuation, has positive changes in both the bandwidth and the S/N ratio, and thereby enhances the resolution of the final processed seismic data.

INTRODUCTION

Seismic attenuation is a fundamental property of subsurface media (Futterman, 1962; Strick, 1970; Kjartansson, 1979). It has a considerable impact on amplitude and wave shape in recorded seismic data. It is of particular importance when seismic attributes and inversion schemes are required to extract lithological information, porosity, permeability, viscosity, and degree of saturation of rocks, because the attenuation parameter is more sensitive than velocity to some of these properties. Attenuation can be quantified in terms of the seismic quality factor *Q*. It is inversely proportional to *Q* and approximately $27.3/Q$ dB per wavelength (Johnston and Toksöz, 1981).

To remove the attenuation effect, inverse *Q* filtering methods have been designed and applied to surface seismic records (Bickel and Natarajan, 1985; Hargreaves and Calvert, 1991; Wang, 2002). A stable and efficient approach to inverse *Q* filtering, proposed in Wang (2002), can recover (1) the distorted phases over the full frequency range and (2) the decayed amplitudes of frequency components up to a recoverable high-frequency limit. This limit is set automatically via the solution stabilization process. This inverse *Q* filtering method is thus referred to as the stabilized approach. In the present paper, I discuss the application of this inverse *Q* filtering method to real seismic data.

To apply inverse *Q* filtering, a reliable estimate of the earth *Q* function is prerequisite. It has been widely accepted that in-situ borehole experiments are best suited for such a reliable estimation (Raikes and White, 1984; Stainsby and Worthington, 1985; Tonn, 1991; Pujol et al., 1998). Dasgupta and Clark (1998) described a method for determining *Q* directly from surface seismic reflection data. Clark et al. (2001) further found that the method worked well in "comparative" circumstances (e.g., time lapse). But most of the time surface seismic data could not provide reliable *Q* values because of contamination of seismic signal by various factors related to data acquisition, such as use of an inadequate source spectrum, offset-dependent tuning of reflections, poor signal-to-noise (S/N) ratio due to multiples and mode conversions, etc. The accuracy of *Q* estimated from downhole seismic is generally higher than that from surface seismic (White, 1992). In this study, I estimate *Q* values from the direct downgoing wavefield of vertical seismic profile (VSP) data.

The *Q* values are estimated using the spectral ratio method. Theoretically, the spectral ratio method will work well with the VSP downgoing wavefield, provided that the following conditions are satisfied: a constant source waveform between upper and lower levels, no interference from reflected waves, the same receiver coupling at upper and lower levels, no variation in stratigraphic filtering between upper and lower levels, and negligible noise in the waveform. In practice, however, the spectral ratios can vary wildly, and the direct application of

Manuscript received by the Editor August 30, 2001; revised manuscript received June 24, 2002.
*Robertson Research International Ltd., Horizon House, Azalea Drive, Swanley, Kent, BR8 8JR, United Kingdom. E-mail: yanghua@geo.robresint.co.uk.

the spectral ratio technique to VSP data can be problematic. The VSP data quality in this paper is even lower than an average level because of poor receiver coupling within some depth ranges. It is obviously a challenge to Q estimation in terms of the robustness of the method.

The estimated Q values are used in designing an inverse Q filter for application to a 2D surface seismic line, which is land seismic with a low S/N ratio relative to marine seismic. A challenge to inverse Q filtering is whether or not the method can improve the S/N ratio without boosting the noise when compensating for both phase and amplitude effects simultaneously. The stabilized inverse Q filtering method and its implementation are described in Wang (2002). In this paper, I focus on the quantitative evaluation of the effectiveness of inverse Q filtering, which corrects for wavelet dispersion in a time-variant manner, compensates for frequency-dependent amplitude decay along the seismic trace, and restores the attenuated frequency components within the signal pass band. These improvements in turn increase the spectral bandwidth and S/N ratio, and hence the resolution of the final processed seismic data.

STABILIZED INVERSE Q FILTERING

Wang (2002) developed a stabilized algorithm for inverse Q filtering, based on the theory of wavefield downward continuation. The method was implemented in a layered manner, assuming a depth-dependent, layered-earth Q model. For each individual constant Q layer, inverse Q filtering consists of two steps. First, the seismic wavefield recorded at the surface was extrapolated down to the top of the current layer. Second, a constant Q inverse filter was applied to the current layer.

In the first step (wavefield extrapolation from the surface to the top of the current layer), instead of applying wavefield downward continuation directly, a reversed, upward continuation system was established. Solving this system produced a stabilized solution.

In the second step (inverse Q filtering within the current constant-Q layer), the amplitude compensation operator, a 2D function of traveltime and frequency, was approximated optimally as the product of two 1D functions depending respectively on time and frequency, and was implemented efficiently in the Fourier domain.

One of the important features of this method is its stability. It can recover all frequency components that in principle are recoverable, and intelligently limit the attempt to compensate a given high-frequency wave component when its amplitude has been attenuated to a level below the ambient noise level. A synthetic example, extracted from Wang (2002), is shown in Figure 1, where (a) shows the synthetic seismic traces showing the effect of earth Q filtering with $Q = 400, 200, 100, 50$ and 25, (b) is the result of a full and exact inverse Q filtering, showing strong artifacts although the synthetic is noise-free, and (c) is the result of the newly developed, stabilized inverse Q filtering approach.

It is apparently the first published method in the geophysical literature which is able to compensate for phase and amplitude simultaneously without boosting the ambient noise. This feature is of significance because seismic resolution is a function of not only the frequency bandwidth but also the S/N ratio. A formula is given later in this paper for measuring the change in seismic resolution.

ROBUST Q ESTIMATION FROM VSP

In this section, I attempt to improve the Q estimation by means of a smooth high-resolution calculation of the spectra, an accurate determination of the time delay, and finally a robust estimation of Q values.

Spectral ratio and time delay

For Q estimation, I use the downgoing wavefield of the VSP data (Figure 2) because it is contaminated the least by other waves and has a relatively high S/N ratio. The amplitude spectrum $A(f)$ of the trace at receiver depth z is assumed to decay exponentially from a reference amplitude $A_0(f)$ at a shallower depth z_0. The decay is measured using the spectral ratio method:

$$\ln\left[\frac{A(f)}{A_0(f)}\right] = -\frac{\pi f(t - t_0)}{Q}, \tag{1}$$

where t and t_0 are the P-wave direct arrival times at depth levels z and z_0, respectively, and f is the frequency. Here Q is assumed to be independent of frequency within the bandwidth (Kjartansson, 1979), and an exponential decay $\exp(-\pi ft/Q)$

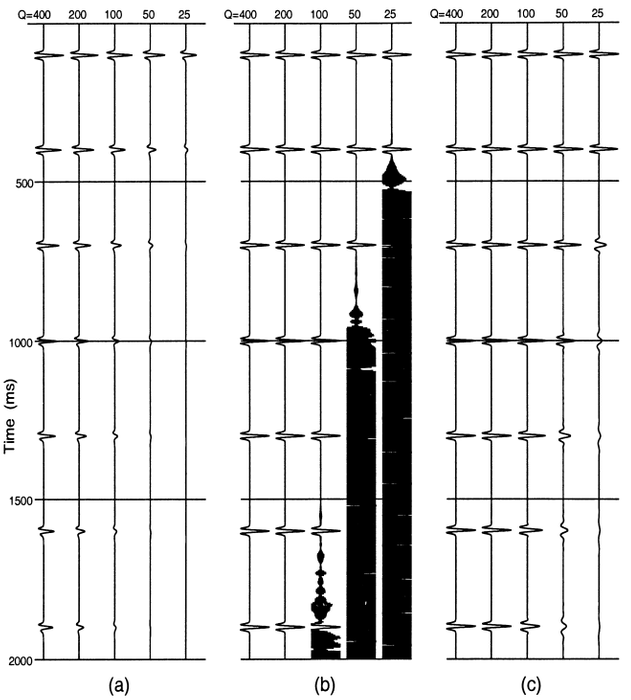

FIG. 1. Earth Q filtering and inverse Q filtering: (a) Synthetic seismic traces which show the effect of earth Q filtering with $Q = 400, 200, 100, 50$ and 25; (b) the result of a full and exact inverse Q filtering, shows strong artifacts, although the synthetic traces are noise-free; (c) the result of stabilized inverse Q filtering approach, which has recovered all frequency components that are in principle recoverable, and has intelligently limited the attempt to compensate a given high-frequency wave component when its amplitude has been attenuated to a level below the ambient noise level.

is used, assuming a small dissipation ($Q > 10$) (Johnston and Toksöz, 1981). Measuring the slope of the spectral ratio

$$k = \frac{1}{f} \ln\left[\frac{A(f)}{A_0(f)}\right], \tag{2}$$

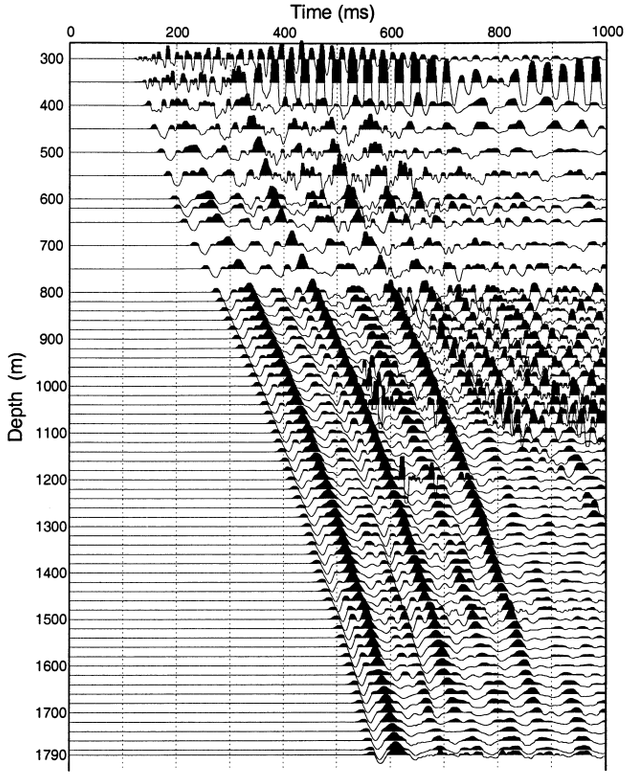

FIG. 2. VSP data recorded at a depth range of 300–1790 m with an irregular depth interval.

and the time delay

$$\tau = t - t_0, \tag{3}$$

the Q value between z_0 and z is then estimated as

$$Q[z_0,\ z] = -\pi\tau/k. \tag{4}$$

In order to calculate the spectral ratio and its logarithm, it is necessary to have a smoothed spectral estimate for each individual waveform, because notches in the amplitude spectrum would cause problems in the spectral division and in the logarithm computation. I here use the multitaper technique to calculate a smooth, high-resolution spectral estimate (Thomson, 1982; Park et al., 1987; Neep, 1995; Riedel and Sidorenko, 1995; Neep et al., 1996). A comparison between the amplitude spectra estimated from the Fourier transform directly and from the multitaper technique is shown in Figure 3, where (a) is a seismic waveform taken from the VSP downgoing wavefield, (b) is the amplitude spectrum estimated directly from the Fourier transform, (c) plots five orthogonal tapers used in the multitaper method, and (d) is the smooth spectrum estimated by the multitaper method.

The orthogonal tapers in Figure 3c are generated numerically, following Thomson (1982) and Park et al. (1987). Each of them is used to provide an orthogonal sample of the original waveform. Fourier transforming these five tapered waveforms generates five corresponding spectra. Finally, a weighted sum of these spectra produces the smooth spectral estimate shown in Figure 3d. Applying the multitaper technique to seismic data would have less spectral leakage than a conventional single taper estimate does (Park et al., 1987).

The slope k [equation (2)] is then estimated by minimizing the absolute deviation between a straight line and the spectral ratio. This algorithm is less affected by large spikes in the spectral ratio than a least-squares algorithm, as the distribution of errors contaminating the data is far from Gaussian.

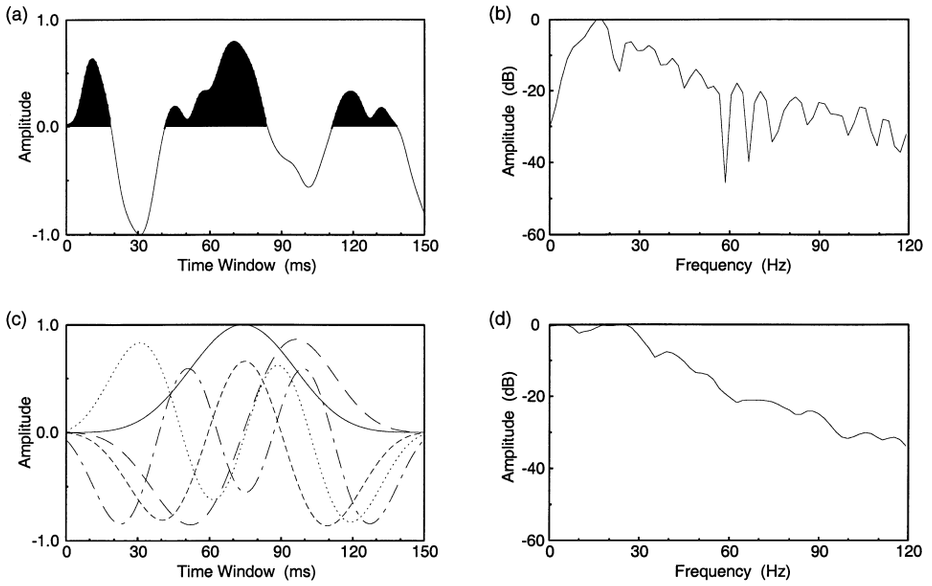

FIG. 3. (a) A first arrival from the VSP data set. (b) The amplitude spectrum estimated directly from the Fourier transform. (c) Five orthogonal tapers. (d) The smooth amplitude spectrum estimated using the multitaper technique.

The time delay τ [equation (3)] is estimated by means of Pearson's correlation coefficient (Molyneux and Schmitt, 1999). Given two waveforms $x_0(t)$ and $x(t)$ (Figure 4a), Pearson's correlation coefficient $r(\tau)$ is measured by

$$r(\tau) = \frac{n\sum_{t=0}^{t=n} x_0(t)x(t+\tau) - \sum_{t=0}^{t=n} x_0(t)\sum_{t=0}^{t=n} x(t+\tau)}{\left(\left[n\sum_{t=0}^{t=n} x_0^2(t) - \left(\sum_{t=0}^{t=n} x_0(t)\right)^2\right] \times \left[n\sum_{t=0}^{t=n} x^2(t+\tau) - \left(\sum_{t=0}^{t=n} x(t+\tau)\right)^2\right]\right)^{\frac{1}{2}}}. \quad (5)$$

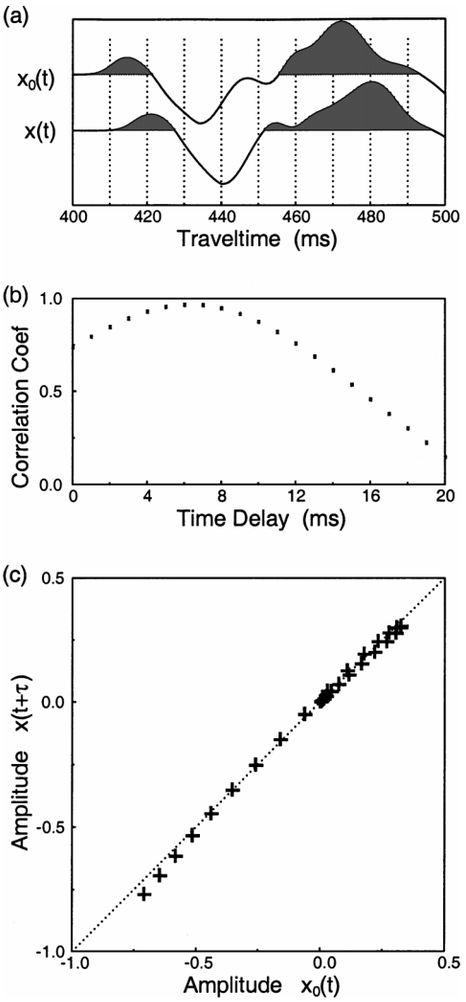

FIG. 4. (a) Two waveforms $x_0(t)$ and $x(t)$ at depths of 1200 and 1220 m, respectively. (b) Pearson's correlation coefficient versus the discrete time shift. The time shift $\tau = 5$ ms at which the correlation coefficient is maximum indicates the most appropriate time delay between the two waveforms. (c) At this time delay τ, the crossplot of the two segments $x_0(t)$ and $x(t+\tau)$ appears linear.

This coefficient is calculated along a series of discrete time shifts (Figure 4b). The τ value at which $r(\tau)$ is maximum indicates the most appropriate time shift. At this time shift, the proximity of $r(\tau)$ to unity suggests a good correlation of shapes between the waveforms $x_0(t)$ and $x(t+\tau)$, and their crossplot appears linear (Figure 4c).

Robust Q estimation

There are many factors affecting the measurement of Q, such as layering effects, reflections and mode conversions, transmission effects, source and receiver coupling effects, spherical divergence, and windowing, as summarized by Pujol and Smithson (1991). Above all, one of the fundamental assumptions in Q estimation is source repeatability. In standard VSP surveys, the source is fired a number of times as the receiver is moved up the well. Changes in the source signature can give rise to apparent changes in frequency content with depth, and thus can cause errors in Q estimates. Such changes should be compensated for whenever possible. If the source signature is recorded, its spectrum can be used to correct the spectra of the downhole recordings by signature deconvolution (Stainsby and Worthington, 1985).

In the case study here, however, such a record of source signature is not available. To overcome the problem associated with variation of source signature between individual shots, I select a reliable Q value from a group of Q estimates calculated for the specific depth. For each depth level z_i, I make several estimates based on the spectral ratios from different depth pairs centered at z_i:

$$\begin{aligned}
Q^{(1)} &= Q[\quad z_{i-1},\ z_i\quad], \\
Q^{(2)} &= Q[\quad z_{i-1},\ z_{i+1}\quad], \\
Q^{(3)} &= Q[z_{i-2},\ z_{i+1}\quad], \\
Q^{(4)} &= Q[z_{i-2},\ z_{i+2}\quad], \\
Q^{(5)} &= Q[z_{i-3},\ z_{i+2}\quad], \\
Q^{(6)} &= Q[z_{i-3},\ z_{i+3}].
\end{aligned}$$

The final Q estimate is given by the following median:

$$\frac{1}{Q(z_i)} = \text{median}\left\{\frac{1}{Q^{(1)}}, \frac{1}{Q^{(2)}}, \ldots, \frac{1}{Q^{(6)}}\right\}. \quad (6)$$

Applying the statistics here, because of scattering in Q estimates due to the non-repeatable source, produces an average Q estimate over a large depth interval. Normally at least one wavelength separation between two receiver depths is needed to be able to measure Q (Raikes and White, 1984; White, 1992).

The estimated Q function is shown in Figure 5, in which the Q function is plotted against the depth and the two-way traveltime. It is interesting to see that the Q function falls considerably when depth increases, typically, at the depth range 1700–1790 m. This Q anomaly can be used in conjunction with other petrophysical attributes as a lithological indicator for seismic interpretion (e.g., McCann et al., 1997).

The smoothed Q function (the dashed line in Figure 5), obtained after applying an arbitrarily chosen five-point median filter, is used in the inverse Q filtering of the surface seismic

data. Below the two-way time 1160 ms (the bottom of the VSP data set), $Q = 100$ is used.

THE EFFECTIVENESS OF INVERSE *Q* FILTERING

Applying the stabilized inverse *Q* filter to surface seismic data would compensate for both phase and amplitude effects simultaneously. In this section, I quantitatively evaluate the effectiveness of this inverse *Q* filtering algorithm.

Figure 6 shows a comparison of the stack section without inverse *Q* filtering and that with inverse *Q* filtering. Random noise attenuation is needed before or after inverse *Q* filtering. I use a technique based on forward-backward spatial prediction (Wang, 1999). It is also necessary to apply a "gap" deconvolution to the data after inverse *Q* filtering. For a fair comparison, both sections in Figure 6 have been processed through these two steps with identical parameters.

Seismic data are generally observed to lose high frequencies with increasing traveltime. The loss of high frequencies lengthens the dominant signal wavelength and thereby degrades the seismic resolution. However, the inverse *Q* filtered section shows a higher dominant frequency than the other one. A time-varying distortion of wavelet phase is evident in the stack section without inverse *Q* filtering. Inverse *Q* filtering has improved the lateral coherence of seismic events, although it is processed trace by trace (for example, see the group of linear events with about 1200 ms intercept time, and two-way time 1000 and 1200 ms at trace 300).

Changes in event times produced by correcting for dispersion are also evident in Figure 6. This is of high importance since it impacts time-to-depth conversion of the seismic (and reservoir) events. But a quantitative comparison is not given in this paper; readers may refer to Hargreaves and Calvert (1991) for some excellent examples. Dispersion-correction-only inverse *Q* filtering is unconditionally stable, however. Difficulties occur only when inverse *Q* filtering includes the energy dissipation correction, which may cause numerical instability and generate undesirable artifacts in the solution. In the present paper, I focus on the stabilized inverse *Q* filtering method, which compensates for both velocity dispersion and energy dissipation simultaneously. Let us now measure the effectiveness quantitatively.

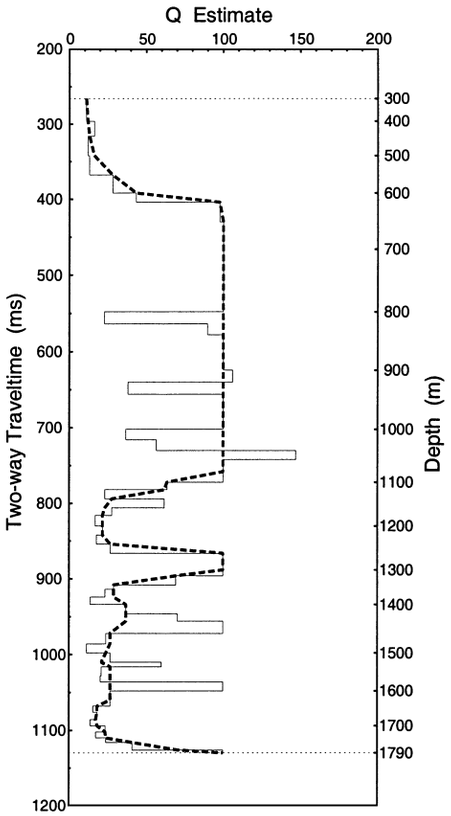

FIG. 5. The *Q* function, estimated from the VSP data, is plotted against the depth and the two-way traveltime. The smoothed function (dashed line), after five-point median filtering, is then used in inverse *Q* filtering of the surface seismic data.

Flattening amplitude spectrum

The amplitude spectra shown in Figure 7 clearly demonstrate that inverse *Q* filtering has flattened the amplitude spectrum within the signal band. The amplitude spectra are computed from an arbitrarily selected trace, number 200. The flattened amplitude spectrum within the band 10–75 Hz indicates an adequate compensation for energy dissipation. It results in a compression of the dispersed wavelet and an increase in phase coherence, as seen in Figure 6. Although the trend of the spectrum has been flattened, the relative amplitude difference between adjacent frequency components is not altered, and thereby the seismic resolution in the frequency axis is kept.

Strengthening relative amplitude

Time-variant amplitude strength, averaged over all traces, is displayed in Figure 8 for different frequency components, in which the dotted and solid lines represent seismic amplitudes without inverse *Q* filtering and with inverse *Q* filtering, respectively. The difference between them reflects the amount of amplitude compensation for different frequency components at different time samples. Generally speaking, inverse *Q* filtering has boosted the relative amplitude strength.

The gray bar drawn as a reference mark in Figure 8 indicates the traveltime ranges within which the amplitude has been fully recovered after inverse *Q* filtering. The stabilized inverse *Q* filter systematically determines such a traveltime range within which a given frequency component is recoverable (as shown in Figure 1). Within the traveltime range, the longer the traveltime is and the higher the frequency is, the more the amplitude has been compensated. Beyond this range, the stabilized inverse *Q* filter reduces the compensation gradually, and we can see the amplitude curves converging. These reference marks are also useful for designing a time-variant band-pass filter, which is essential especially for land seismic processing.

Increasing spectral bandwidth

The statistical bandwidth is estimated using the method of Walden and White (1990) as

$$\hat{B} = \frac{\phi_0^2}{2\sum_{\tau=-(T-1)}^{T-1}\left(1-\frac{|\tau|}{T}\right)w_\tau^2\phi_\tau^2}, \qquad (7)$$

where $\phi_\tau = (1/T)\sum x_t x_{t+\tau}$ is the sample autocovariance constructed from the time series $\{x_1, x_2, \ldots, x_T\}$, T is the duration of the data segment, and w_τ is a taper window. It is then corrected to give approximately an unbiased estimate:

$$B = \left(1 + \frac{2}{\nu}\right)\hat{B} - \frac{1}{T}, \tag{8}$$

where ν is the number of degrees of freedom associated with w_τ.

Figure 9 shows the time-variant bandwidth estimate (averaged over all the traces shown in Figure 6) of the seismic data without inverse Q filtering (dotted line) and using inverse Q filtering (solid line). It indicates clearly that inverse Q filtering has increased the seismic temporal bandwidth by 15–20 Hz.

Improving S/N ratio

The S/N power ratio of a specific trace $x_{k,t}$, among a set of $q+1$ traces, is estimated by (White, 1980, 1984; Walden and White, 1984)

$$\hat{\rho}_k(f) = \frac{\left|\underline{\Phi}_{qk}^{\dagger}(f)\underline{\underline{\Phi}}_{qq}^{-1}(f)\underline{\Phi}_{qk}(f)\right|}{\left|\Phi_{kk|q}(f)\right|}, \tag{9}$$

where f is the frequency, $\underline{\underline{\Phi}}_{qq}^{-1}$ is the inverse of the spectral matrix of the q traces, $\underline{\Phi}_{qk}$ is the column vector of their cross

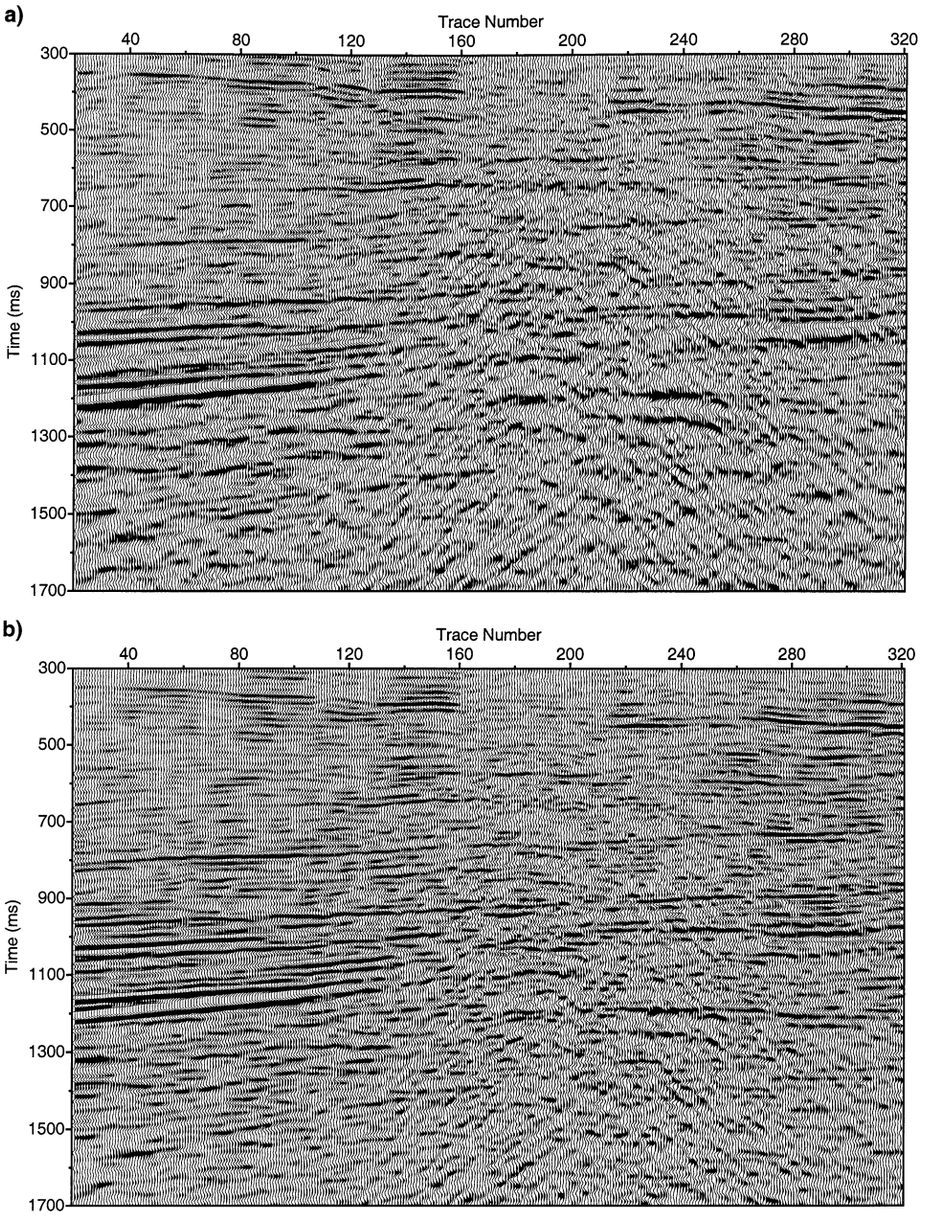

FIG. 6. Comparison of a stack section without inverse Q filtering (a) and one after applying stabilized inverse Q filtering (b).

spectra with the trace $x_{k,t}$, $\underline{\Phi}^{\dagger}_{qk}$ is its conjugate transpose, and $\Phi_{kk|q}$ is the estimated noise power on $x_{k,t}$, defined as the spatially unpredictable energy:

$$\Phi_{kk|q}(f) = \Phi_{kk}(f) - \underline{\Phi}^{\dagger}_{qk}(f)\underline{\underline{\Phi}}^{-1}_{qq}(f)\underline{\Phi}_{qk}(f). \qquad (10)$$

For each specific trace $x_{k,t}$, we have $q+1$ estimates $\hat{\rho}^{(j)}_k$, for $j=1,\ldots q+1$. Each individual $\hat{\rho}^{(j)}_k$ is estimated from one of the following trace groups, $\{x_{k-q,t},\ldots,x_{k,t}\}$, $\{x_{k-q+1,t},\ldots,x_{k+1,t}\},\ldots,\{x_{k,t},\ldots,x_{k+q,t}\}$, each consisting of $q+1$ traces. The final measurement $\hat{\rho}_k$ is the average of these $q+1$ estimates $\{\hat{\rho}^{(j)}_k\}$. In the example, $q=3$ is used.

Figure 10 displays the S/N ratios of a seismic trace (number 200) within four different time windows. The S/N ratio improvement varies within different time windows, with significant improvement on the shallow portion. In the shallow portion, the S/N ratio improvement is up to 75 Hz. In the middle and deep portions, this upper limit decreases gradually. This phenomenon is consistent with the experiment shown in Figure 1, in that the stabilized inverse *Q* filtering method automatically determines recoverable frequency components according to the travel distance or time.

Enhancing seismic resolution

The spectral bandwidth and the S/N ratio are related to the seismic resolution. Let us now define an empirical formula to measure the resolution enhancement quantitatively.

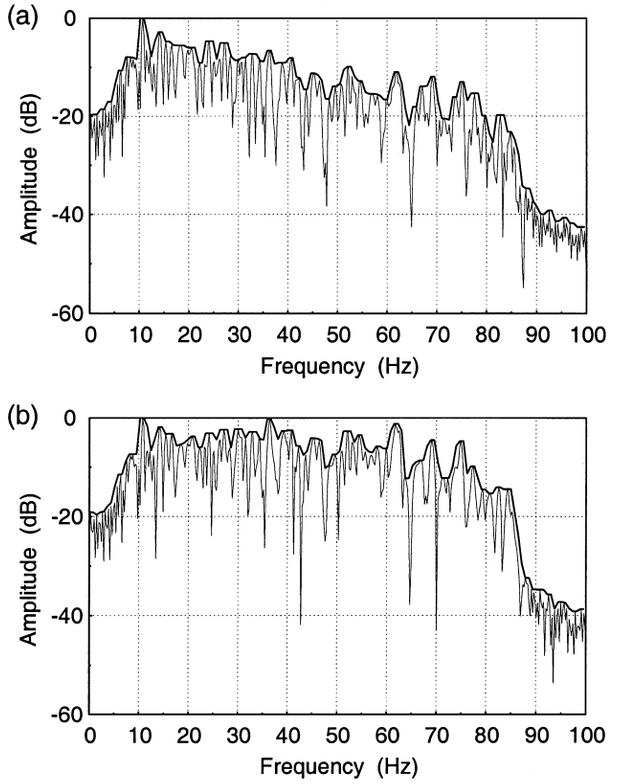

FIG. 7. Comparison of the amplitude spectra of a stack trace (number 200) without inverse *Q* filtering (a) and using inverse *Q* filtering (b). The two lines in each spectrum plot are the DFT result and the median-filtered smooth spectrum, respectively.

The standard deviation of the time-shift estimate τ, on which our formula is based, may be evaluated as (White and Harris, 1993)

$$\mathrm{var}\{\tau\} = \frac{3}{2\pi^2(B^2-b^2)BT}\left(\frac{1}{\gamma^2}-1\right), \qquad (11)$$

where b is the bandwidth of the spectral window employed in the analysis, and γ^2 is the spectral coherence. The spectral coherence measures the predictability of one trace from the other (White, 1973; 1984) and is frequency dependent. I estimate it here approximately by

$$\hat{\gamma}^2(f) = \frac{\hat{\rho}^2(f)}{[1+\hat{\rho}(f)]^2}, \qquad (12)$$

where $\hat{\rho}(f)$ is the average of the S/N ratio $\hat{\rho}_k(f)$ over all the traces. The γ^2 value in equation (11) is the average of $\hat{\gamma}^2(f)$ over the frequency band.

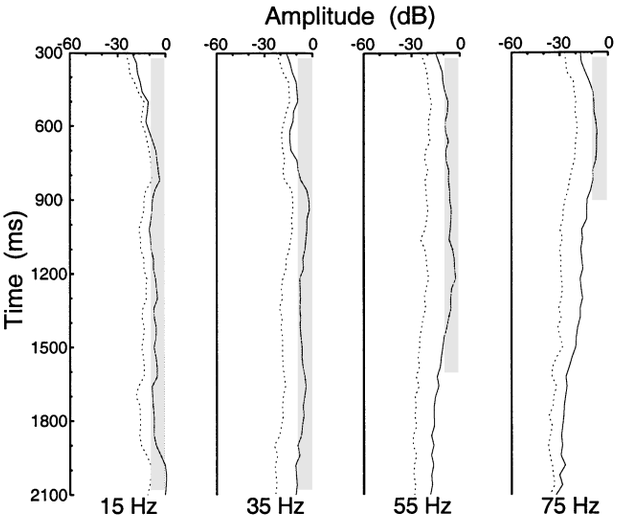

FIG. 8. Comparison of the time-variant amplitude strength (averaged over all traces shown in Figure 6) of different frequency components without inverse *Q* filtering (dotted lines) and with inverse *Q* filtering (solid lines). The gray bar drawn as a reference mark indicates the portion of the data set within which the amplitude has been fully recovered after inverse *Q* filtering.

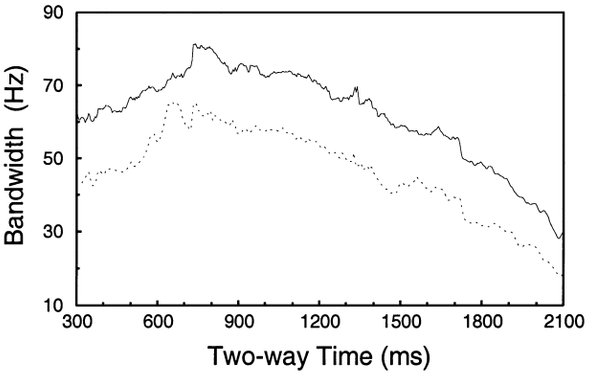

FIG. 9. Comparison of the time-variant bandwidth estimate (averaged over all traces shown in Figure 6) of the seismic data without inverse *Q* filtering (dotted line) and with inverse *Q* filtering (solid line).

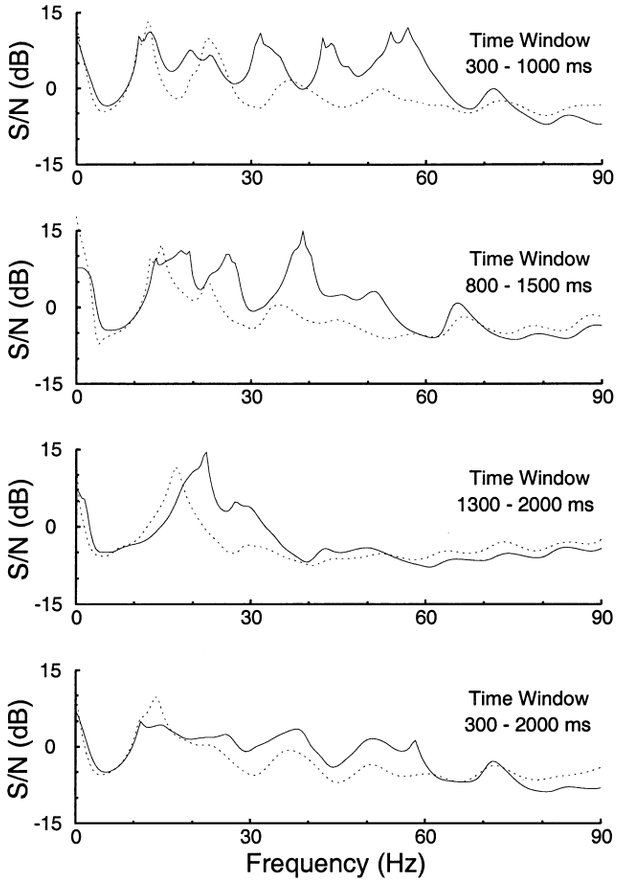

FIG. 10. Comparison of the S/N ratios of a seismic trace (number 200) without inverse Q filtering (dotted lines) and with inverse Q filtering (solid lines). The S/N improvement varies within different time windows.

Defining a parameter δ to measure the resolution enhancement as

$$\delta = -\frac{\Delta(\mathrm{var}\{\tau\})}{\mathrm{var}\{\tau\}}, \tag{13}$$

represented in terms of the (negative) change of the standard deviation of the time shift, I obtain the following expressions:

$$\delta = \left(3 + \frac{2b^2}{B^2 - b^2}\right)\frac{\Delta B}{B} + \left(1 + \frac{1}{1+2\rho}\right)\frac{\Delta\rho}{\rho} \tag{14}$$

$$\approx 3\frac{\Delta B}{B} + 2\frac{\Delta\rho}{\rho}, \tag{15}$$

where the relative increment of the spectral bandwidth, $\Delta B/B$, is the average value over the time window, and the relative increment in the S/N ratio, $\Delta\rho/\rho$, is the average value over the frequency band.

The improvements (in percentage) on spectral bandwidth, S/N ratio, and the temporal resolution within different time windows are summarized in Table 1. It is worthwhile to notice that overall within the time range 300–2000 ms, we have a 36% increment in spectral bandwidth, a 27% increment in the S/N ratio, and a 162% enhancement in temporal resolution.

Table 1. Relative improvements (in percentage) on spectral bandwidth ($\Delta B/B$), S/N ratio ($\Delta\rho/\rho$), and the temporal resolution (δ).

Time (ms)	$\Delta B/B$ (%)	$\Delta\rho/\rho$ (%)	δ (%)
300–1000	30	82	254
800–1500	32	56	208
1300–2000	42	16	158
300–2000	36	27	162

CONCLUSIONS

The surface seismic data processed with the stabilized inverse Q filtering method have shown significant improvement over the data processed without inverse Q filtering. The process of inverse Q filtering has flattened the amplitude spectrum, strengthened the time-variant amplitude, increased the spectral bandwidth, improved the S/N ratio, and hence enhanced the seismic resolution of the final processed seismic data set.

A parameter defined to measure the resolution enhancement is a function of the changes in the bandwidth and the S/N ratio. A problem with conventional full inverse Q filtering methods is that they may increase the bandwidth but degrade the S/N ratio, and thus may not improve the resolution. However, the stabilized inverse Q filtering algorithm may have positive changes in both the bandwidth and S/N ratio, and in turn enforce the seismic resolution improvement.

ACKNOWLEDGMENTS

The author sincerely acknowledges Professor Roy White for a detailed explanation of his previous publications on the spectral coherence method, Damian Ainscough for his kind assistance in providing the seismic data, and Stuart Merrylees for his support to this project. Data processing was conducted by Simon Evans and Kevin Harber, Land Seismic Department, Robertson Research International.

REFERENCES

Bickel, S. H., and Natarajan, R. R., 1985, Plane-wave Q-deconvolution: Geophysics, **50**, 1426–1439.
Clark, R. A., Carter, A. J., Nevill, P. C., and Benson, P. M., 2001, Attenuation measurements from surface seismic data—Azimuthal variation and time-lapse case studies: 63rd Conf., Eur. Assn. Geosci. Eng., Extended Abstracts, L-28.
Dasgupta, R., and Clark, R. A., 1998, Estimation of Q from surface seismic reflection data: Geophysics, **63**, 2120–2128.
Futterman, W. I., 1962, Dispersive body waves: J. Geophys. Res., **69**, 5279–5291.
Hargreaves, N. D., and Calvert, A. J., 1991, Inverse Q filtering by Fourier transform: Geophysics, **56**, 519–527.
Johnston, D. H., and Toksöz, M, N., 1981, Definitions and terminology, *in* Toksöz, M, N., and Johnston, D. H., eds., Seismic wave attenuation: Soc. Expl. Geophys., 1–5.
Kjartansson, E., 1979, Constant Q wave propagation and attenuation: J. Geophys. Res., **84**, 4737–4748.
McCann, C., Sothcott, J., and Assefa, S. B., 1997, Prediction of petrophysical properties from seismic quality factor measurements, *in* Lovell, M. A., and Harvey, P. K., eds., Development in Petrophysics: Geological Society Special Publication, **122**, 121–130.
Molyneux, J. B., and Schmitt, D. R., 1999, First-break timing—Arrival onset times by direct correlation: Geophysics, **64**, 1492–1501.
Neep, J., 1995, Robust estimation of P-wave attenuation from full waveform array sonic data: J. Seismic Expl., **4**, 329–344.
Neep, J. P., Sams, M. S., Worthington, M. H., and O'Hara-Dhand, K. A., 1996, Measurement of seismic attenuation from high-resolution crosshole data: Geophysics, **61**, 1175–1188.
Park, J., Lindberg, C. R., and Vernon, F. L., 1987, Multitaper spectral analysis of high frequency seismograms: J. Geophys. Res., **92**, 12675–12684.

Pujol, J., and Smithson, S., 1991, Seismic wave attenuation in volcanic rocks from VSP experiments: Geophysics, **56**, 1441–1455.
Pujol, J. M., Luschen, E., and Hu, Y., 1998, Seismic wave attenuation in metamorphic rocks from VSP data recorded in Germany's continental super-deep borehole: Geophysics, **63**, 354–365.
Raikes, S. A., and White, R. E., 1984, Measurements of earth attenuation from downhole and surface seismic recordings: Geophys. Prosp., **32**, 892–919.
Riedel, K. S., and Sidorenko, A., 1995, Minimum bias multiple taper spectral estimation: IEEE Trans. Signal Proc., **43**, 188–195.
Stainsby, S. D., and Worthington, M. H., 1985, *Q* estimation from vertical seismic profile data and anomalous variations in the central North Sea: Geophysics, **50**, 615–626.
Strick, E., 1970, A predicted pedestal effect for pulse propagation in constant-*Q* solids: Geophysics, **35**, 387–403.
Thomson, D. J., 1982, Spectrum estimation and harmonic analysis: Proc. IEEE, **70**, 1055–1096.
Tonn, R., 1991, The determination of the seismic quality factor *Q* from VSP data—A comparison of different computational methods: Geophys. Prosp., **39**, 1–28.
Walden, A. T., and White, R. E., 1984, On errors of fit and accuracy in matching synthetic seismograms and seismic traces: Geophys. Prosp., **32**, 871–891.
——— 1990, Estimating the statistical bandwidth of a time series: Biometrika, **77**, 699–707.
Wang, Y., 1999, Random noise attenuation using forward-backward linear prediction: J. Seismic Expl., **8**, 133–142.
——— 2002, A stable and efficient approach of inverse *Q* filtering: Geophysics, **67**, 657–663.
White, R. E., 1973, The estimation of signal spectra and related quantities by means of the multiple coherence function: Geophys. Prosp., **21**, 660–703.
——— 1980, Partial coherence matching of synthetic seismograms with seismic traces: Geophys. Prosp., **28**, 333–358.
——— 1984, Signal and noise estimation from seismic reflection data using spectral coherence methods: Proc. IEEE, **72**, 1340–1356.
——— 1992, The accuracy of estimating *Q* from seismic data: Geophysics, **57**, 1508–1511.
White, R. E., and Harris, P. E., 1993, Phase and timing accuracy: Birkbeck College, University of London, Research Note.